14 Time-Optimal Path Planning for the General Waiter Motion Problem

Francisco Geu Flores and Andrés Kecskeméthy

Dedicated to Professor Ken Waldron on occasion of his 70th birthday.

Abstract. This paper presents a direct solution approach for the so-called general waiter motion problem, which consists in moving a tablet as fast as possible from one pose to the other such that non of the objects resting on the tablet slides at any time. The question is akin to several industrial problems in which tangential forces are restricted due to functional reasons, such as suction grippers, motion of sensitive goods, etc. In contrast to existing approaches which parametrize the problem in configuration (joint) space, we decompose the overall task into two cascaded main components: shaping the optimal geometry of the spatial path, and finding the time optimal one-dimensional motion of the system along this path. The spatial path is parametrized using via poses in SE(3), making it possible to reduce the search space to significant physical subspaces, and to interact intuitively with the user. The overall optimization is subdivided into a series of subproblems with cost functions and search spaces of increasing fineness, such that each subproblem can be solved with the output of its predecessor. A solution of the waiter motion problem with four objects illustrates the applicability of the algorithm.

1 Problem Statement

Discussed in this paper is a solution procedure to the so-called general waiter motion problem, which consists in computing the time-optimal motion of a six-degrees-of-freedom manipulator carrying a tablet with an arbitrary number of objects resting on it from an initial pose $\mathscr{K}_{\mathrm{E}0}$ to a final pose $\mathscr{K}_{\mathrm{E}f}$ as fast as possible, such that non of the objects slides at any time (see Fig. 1). This problem is akin to (offline) motion planning problems in which tangential forces at contacts are restricted due

Francisco Geu Flores · Andrés Kecskeméthy
Lehrstuhl für Mechanik und Robotik, Universität Duisburg-Essen,
Lotharstr. 1, 47057 Duisburg, Germany
e-mail: {francisco.geu,andres.kecskemethy}@uni-due.de

V. Kumar et al. (Eds.): *Adv. in Mech., Rob. & Des. Educ. & Res.*, MMS 14, pp. 189–203.
DOI: 10.1007/978-3-319-00398-6_14 © Springer International Publishing Switzerland 2013

to functional constraints (e.g. suction grippers, motion of sensitive goods). Most state-of-the-art motion planning algorithms use spline functions in *configuration coordinates* (i.e., robot joint coordinates) to transform the optimal control problem into a nonlinear optimization problem [1]. Hereby, the spline domain is defined either as a linear mapping of the cycle time [1] — which allows for a direct search of the optimal time intervals between the inner spline knots — or as a general spline parameter decoupled from time [2] — which requires the additional computation of the optimal time history of the spline parameter for a given set of spline coefficients and knots. However, such algorithms display difficulties to converge for coupled shape/time optimality problems such as the one presented in this paper, mainly because the overall optimization problem's extreme nonlinearity causes the optimizer to remain trapped in local minima or even in infeasible regions.

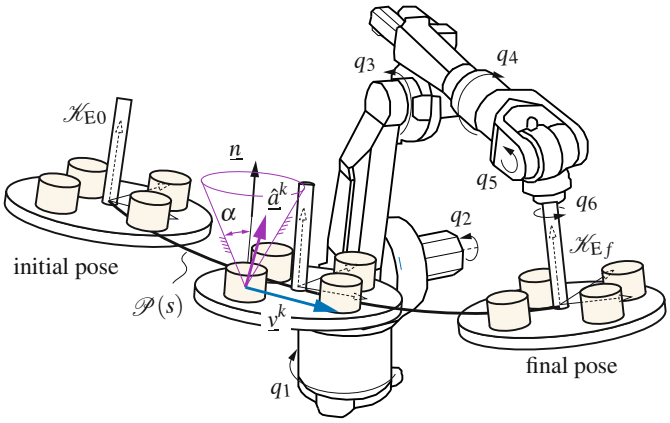

Fig. 1 General waiter-motion problem

In this paper, we propose a novel procedure for coupled shape/time optimality problems by (1) using target (i.e. task space) coordinates instead of configuration coordinates and (2) parametrizing the spline shape functions in terms of via-poses instead of using the spline coefficients and knots. This allows for optimizing over a more natural function basis and for restricting the search space during optimization to significant subspaces. Hence, the condition of the optimization problem is improved and less and computationally cheaper iterations are required for convergence. To this end, the robot's motion is decomposed in two cascaded main components: the spatial path $\mathscr{P}(s) \in \mathrm{SE}(3)$ traversed by the robot end-effector (the tablet) $\mathscr{K}_{\mathrm{E}}$, and the one-dimensional motion $s(t)$ of the tablet along this path, where s denotes the path coordinate along the curve described by $\mathscr{K}_{\mathrm{E}}$. The spatial path $\mathscr{P}(s)$ is parametrized using fifth and third-order fitted B-splines for translation and rotation, respectively, and the motion $s(t)$ along the path is computed by solving the time-optimal problem using the well-known and classical methods of robotics

developed by [3], [4] and [5]. In order to warrant convergence, the overall optimal control problem is formulated as a sequence of nonlinear optimization problems of increasing fineness, such that each subproblem takes the solution of its predecessor as initial guess. Hereby, each subproblem is solved by standard gradient-based optimization routines. This shows that the decomposition of the problem into spatial shape and time-optimal motion is instrumental in finding the coupled shape/time optimal solution. The proposed method can be used to handle a broad spectrum of applications, ranging from optimal roller-coaster design up to minimal-cycle-time excavator operations under power constraints ([6], [7]).

The rest of the paper is organized as follows. Section 2 describes the model of a spatial path as a kinetostatic transmission element – termed "curved joint" – transmitting motion and forces. In Section 3, the time-optimal problem along a specified trajectory is solved using an extension of the well-known methods from robotics ([3], [4], [5]) to general multibody systems, which is easily possible due to the employed object-oriented approach. Section 4 finally describes the application of the developed methods to a 4-object waiter motion problem and the solutions obtained.

2 Generic Properties of Spatial Paths in Multibody Systems

Let a general spatial path be given by the pose of an output frame $\mathscr{K}_\mathrm{E} = \mathscr{P}(s) \in \mathrm{SE}(3)$, with the translation part of $\mathscr{P}(s)$ described by a vector $\Delta\underline{r}(s)$ and the rotation part parametrized by a rotation matrix $\Delta\mathbf{R}(s)$, both measured with respect to a basis frame $\mathscr{K}_1$. Let the coordinate s be the path length of the spatial curve followed by $\mathscr{K}_\mathrm{E}$, as shown in Fig. 2.

The pose of $\mathscr{K}_\mathrm{E}$ can be computed as a function of the pose of the basis frame $\mathscr{K}_1$ and the path coordinate s as

$$\begin{aligned} {}^0\mathbf{R}_\mathrm{E} &= {}^0\mathbf{R}_1\,\Delta\mathbf{R}\,, && \text{with} \quad \Delta\mathbf{R} = \Delta\mathbf{R}(s) \\ \underline{r}_\mathrm{E} &= \Delta\mathbf{R}^\mathrm{T}\left(\underline{r}_1 + \Delta\underline{r}\right), && \text{with} \quad \Delta\underline{r} = \Delta\underline{r}(s)\,. \end{aligned} \tag{1}$$

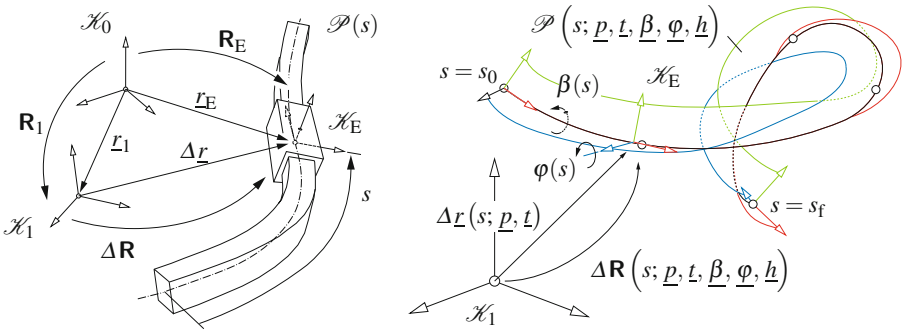

Fig. 2 Curve joint as a kinetostatic transmission element ([8])

The angular and linear absolute velocities of $\mathscr{K}_\mathrm{E}$ can be computed as

$$\underline{\mathrm{t}}_\mathrm{E} = \begin{bmatrix} \underline{\omega}_\mathrm{E} \\ \underline{v}_\mathrm{E} \end{bmatrix} = \underbrace{\begin{bmatrix} \Delta\mathbf{R}^\mathrm{T} & \underline{0} \\ -\Delta\mathbf{R}^\mathrm{T}\widetilde{\Delta\underline{r}} & \Delta\mathbf{R}^\mathrm{T} \end{bmatrix}}_{\mathbf{J}_g} \begin{bmatrix} \underline{\omega}_1 \\ \underline{v}_1 \end{bmatrix} + \mathbf{J}_\mathscr{P}\,\dot{s}, \tag{2}$$

where $\mathbf{J}_g$ is the rigid-body Jacobian, and $\mathbf{J}_\mathscr{P}$ is the Jacobian mapping the path velocity $\dot{s}$ along the spatial path to the twist $\underline{\mathrm{t}}_\mathrm{E}$ at the output frame $\mathscr{K}_\mathrm{E}$.

The angular and linear absolute accelerations of $\mathscr{K}_\mathrm{E}$ can be computed as

$$\dot{\underline{\mathrm{t}}}_\mathrm{E} = \begin{bmatrix} \dot{\underline{\omega}}_\mathrm{E} \\ \underline{a}_\mathrm{E} \end{bmatrix} = \mathbf{J}_g \begin{bmatrix} \dot{\underline{\omega}}_1 \\ \underline{a}_1 \end{bmatrix} + \begin{bmatrix} \underline{0} \\ {}^2\widetilde{\underline{\omega}}_1^2\Delta\mathbf{R}^\mathrm{T}\Delta\underline{r} \end{bmatrix} + \mathbf{J}_\mathscr{P}\,\ddot{s} + \mathbf{J}_\mathscr{P}'\,\dot{s}^2 + \begin{bmatrix} {}^2\widetilde{\underline{\omega}}_1 & \mathbf{0} \\ \mathbf{0} & 2\,{}^2\widetilde{\underline{\omega}}_1 \end{bmatrix} \mathbf{J}_\mathscr{P}\,\dot{s}, \tag{3}$$

where $(.)'$ denotes the derivative with respect to the path coordinate s.

Furthermore, the duality of velocity and force transmission yields

$$\begin{bmatrix} \underline{\tau}_1 \\ \underline{f}_1 \\ Q_s \end{bmatrix} = \begin{bmatrix} \mathbf{J}_g^\mathrm{T} \\ \mathbf{J}_\mathscr{P}{}^\mathrm{T} \end{bmatrix} \begin{bmatrix} \underline{\tau}_\mathrm{E} \\ \underline{f}_\mathrm{E} \end{bmatrix}, \tag{4}$$

where $\underline{\tau}_1$, $\underline{f}_1$ are the torque and force at frame $\mathscr{K}_1$ and $\underline{f}_1$ is the force projected along $\mathscr{P}(s)$. The functions $\Delta\underline{r}(s)$, $\Delta\mathbf{R}(s)$, and $\mathbf{J}_\mathscr{P}$ depend on the description of the spatial path $\mathscr{P}(s)$.

In this work, the parametrization $\Delta\underline{r}(s)$ of the spatial curve is computed by interpolating relative via-positions of the origin of the output frame $\mathscr{K}_\mathrm{E}$ with respect to the input frame $\mathscr{K}_1$ using smoothing splines with end-point derivative constraints (curve-fitting routine `concur` [9]). The orientation of frame $\mathscr{K}_\mathrm{E}$ with respect to $\mathscr{K}_1$, i. e. the rotation matrix $\Delta\mathbf{R}(s)$, is prescribed by means rotations about the tangential and normal directions of a DARBOUX frame ([8]), as shown in Fig. 2. In the figure, the via-points are collected in vector $\underline{p}$, the boundary conditions of $\Delta\underline{r}(s)$ are collected in vector $\underline{t}$, the horizon via-vectors are collected in vector $\underline{h}$, and the via-angles in tangential and normal directions are collected in vectors $\underline{\beta}$ and $\underline{\varphi}$, respectively.

3 Time-Optimal Motion Along a Given Spatial Path

3.1 Formulation of the Time-Optimal Problem

Let $\underline{\varphi}_q$ represent the direct kinematics of a multibody system consisting of r massive rigid bodies, p dependent joint coordinates β_j, n independent joint coordinates q_i, collected in the vector $\underline{q} \in \mathbf{R}^n$, as well as an end effector frame $\mathscr{K}_\mathrm{E}$, as shown in Fig. 3. Let the spatial motion of the multibody system be given in target coordinates $\mathscr{K}_\mathrm{E} = \mathscr{P}(s) \in \mathrm{SE}(3)$ as a function of a the path coordinate s. The configuration of the system is uniquely defined by s, and its state is uniquely defined by the vector $[s, \dot{s}]^\mathrm{T}$. If all configurations $\mathscr{P}(s)$ are reachable, both system and spatial path can be

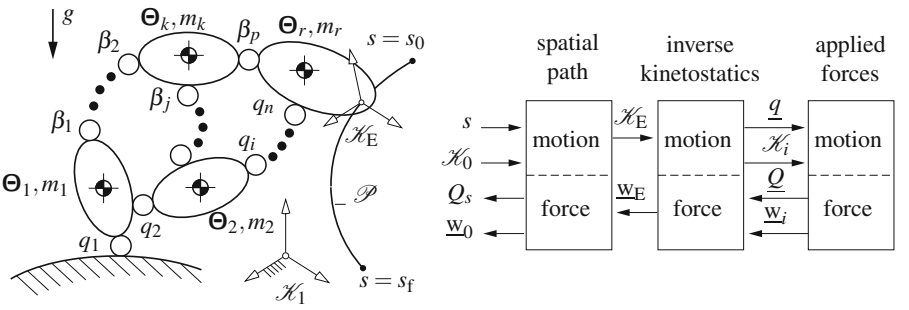

Fig. 3 Multibody system performing a task along the spatial path $\mathscr{P}$

regarded as a single kinetostatic transmission element mapping the path coordinate s to the joint motion $\underline{q}$ and end-effector motion $\mathscr{K}_E$ (see Fig. 3).

The corresponding joint motion is hereby described by the equations

$$\begin{aligned}
\underline{q} &= \underline{\varphi}_q{}^{-1}(\mathscr{P}(s)) \\
\dot{\underline{q}} &= \mathbf{J}_\varphi{}^{-1}\mathbf{J}_\mathscr{P}\dot{s} \\
\ddot{\underline{q}} &= \mathbf{J}_\varphi{}^{-1}\mathbf{J}_\mathscr{P}\ddot{s} + \left[\mathbf{J}'_\varphi{}^{-1}\mathbf{J}_\mathscr{P} + \mathbf{J}_\varphi{}^{-1}\mathbf{J}'_\mathscr{P}\right]\dot{s}^2,
\end{aligned} \tag{5}$$

where $\mathbf{J}_\varphi = \partial\underline{\varphi}_q/\partial\underline{q}$ represents the transmission Jacobian of the multibody system. The prescribed spatial path $\mathscr{P}(s)$ as well as its corresponding Jacobian $\mathbf{J}_\mathscr{P}$ describe the kinematical transmission of a curve joint as presented in Sect. 2.

The velocities and accelerations at the independent joints and at the end-effector have the general form

$$\begin{aligned}
\dot{\underline{q}} &= {}_q\mathbf{J}_s\,\dot{s}, & \ddot{\underline{q}} &= {}_q\mathbf{J}_s\,\ddot{s} + {}_q\mathbf{J}'_s\,\dot{s}^2, \\
\underline{t}_E &= {}_E\mathbf{J}_s\,\dot{s}, & \dot{\underline{t}}_E &= {}_E\mathbf{J}_s\,\ddot{s} + {}_E\mathbf{J}'_s\,\dot{s}^2,
\end{aligned} \tag{6}$$

Let now the dynamics of the multibody system be described by the differential equations in minimal form

$$\mathbf{M}(\underline{q})\ddot{\underline{q}} + \underline{b}(\underline{q},\dot{\underline{q}}) - \underline{Q}_e(\underline{q},\dot{\underline{q}}) - \underline{Q}_G(\underline{q}) = \underline{Q}, \tag{7}$$

where $\mathbf{M}$ is the $n \times n$ mass matrix of the multibody system, $\underline{b}(\underline{q},\dot{\underline{q}})$ is the n-dimensional vector containing the centripetal and Coriolis terms, $\underline{Q}_G(\underline{q})$ is an n-dimensional vector containing the projection of the gravitational forces on the generalized coordinates, $\underline{Q}_e(\underline{q},\dot{\underline{q}})$ is an n-dimensional vector containing the projection of general external forces, and $\underline{Q}$ is an n-dimensional vector collecting the generalized actuator forces.

Let the velocities $\dot{\underline{q}}$, accelerations $\ddot{\underline{q}}$, and generalized actuator forces $\underline{Q}$ at the joints be constrained by equations of the form

$$\begin{aligned} \underline{\dot{q}}^{\min}(\underline{q}) \le \underline{\dot{q}} \le \underline{\dot{q}}^{\max}(\underline{q}) \\ \underline{\ddot{q}}^{\min}(\underline{q},\underline{\dot{q}}) \le \underline{\ddot{q}} \le \underline{\ddot{q}}^{\max}(\underline{q},\underline{\dot{q}}) \\ \underline{Q}^{\min}(\underline{q},\underline{\dot{q}}) \le \underline{Q} \le \underline{Q}^{\max}(\underline{q},\underline{\dot{q}}), \end{aligned} \tag{8}$$

and the velocities $\underline{\mathrm{t}}_{\mathrm{E}}$ and accelerations $\dot{\underline{\mathrm{t}}}_{\mathrm{E}}$ at the end-effector be constrained by equations of the form

$$\begin{aligned} \underline{\mathrm{t}}_{\mathrm{E}}^{\min}(\mathscr{K}_{\mathrm{E}}) \le \underline{\mathrm{t}}_{\mathrm{E}} \le \underline{\mathrm{t}}_{\mathrm{E}}^{\max}(\mathscr{K}_{\mathrm{E}}) \\ \dot{\underline{\mathrm{t}}}_{\mathrm{E}}^{\min}(\mathscr{K}_{\mathrm{E}},\underline{\mathrm{t}}_{\mathrm{E}}) \le \dot{\underline{\mathrm{t}}}_{\mathrm{E}} \le \dot{\underline{\mathrm{t}}}_{\mathrm{E}}^{\max}(\mathscr{K}_{\mathrm{E}},\underline{\mathrm{t}}_{\mathrm{E}}). \end{aligned} \tag{9}$$

With the relations Eq. 6, the equations of motion described in Eq. 7 can be written in terms of the motion coordinate s as

$$\underline{m}(s)\ddot{s} + \underline{c}(s,\dot{s}) + \underline{d}(s) = \underline{Q}, \tag{10}$$

with $\underline{m}(s) = \mathbf{M}(s)_q \mathbf{J}_s$, $\underline{c}(s,\dot{s}) = \left[\mathbf{M}(s)_q \mathbf{J}'_s + \bar{\underline{b}}(s)\right]\dot{s}^2 - \underline{Q}_{\mathrm{e}}(s,\dot{s})$, and $\underline{d}(s) = -\underline{Q}_{\mathrm{G}}(s)$, where the components m_i and c_i of vectors $\underline{m}$ and $\underline{c}$ represent the effective inertia and velocity forces at every independent joint, respectively, and the term $\underline{b}(\underline{q},\underline{\dot{q}})$ in Eq. 7 can be written as $\bar{\underline{b}}(s)\,\dot{s}^2$, with $\bar{\underline{b}}(s)$ depending only on the configuration s.

Furthermore, Eq. 6 allows for all constraints of the form Eq. 8 and Eq. 9 to be collected in the vector inequality

$$\hat{\underline{b}}_1(s,\dot{s}) \le \hat{\underline{m}}(s)\,\ddot{s} \le \hat{\underline{b}}_2(s,\dot{s}), \tag{11}$$

where $\hat{\underline{b}}_1$, $\hat{\underline{b}}_2$ and $\hat{\underline{m}}$ are vectors in $\mathbf{R}^l$ and l is the number of constraints.

The left and right sides of this inequality define the set of admissible states $[s,\dot{s}]^{\mathrm{T}}$ and can be written compactly as the scalar inequality

$$G(s,\dot{s}) \le 0, \tag{12}$$

with $G(s,\dot{s}) = \max\left\{\hat{b}_{1j}(s,\dot{s}) - \hat{b}_{2j}(s,\dot{s})\right\}$, for all $j = 1,2,\cdots,\ell$.

For all constraints j for which $\hat{m}_j(s)$ does not vanish, Eq. 11 further limits the acceleration $\ddot{s}$ along the spatial path, since it must hold

$$\frac{\hat{b}_{1j}(s,\dot{s})}{|\hat{m}_j(s)|} \le \operatorname{sgn}\left[\hat{m}_j(s)\right]\ddot{s} \le \frac{\hat{b}_{2j}(s,\dot{s})}{|\hat{m}_j(s)|}, \tag{13}$$

or compactly $l_j(s,\dot{s}) \le \ddot{s} \le u_j(s,\dot{s})$, where $l_j(s,\dot{s})$ and $u_j(s,\dot{s})$ are the lower and upper bounds of the j-th constraint, functions of the state $[s,\dot{s}]^{\mathrm{T}}$. These equations can be rewritten as the one dimensional inequality

$$L(s,\dot{s}) \le \ddot{s} \le U(s,\dot{s}), \tag{14}$$

where $L(s,\dot{s}) = \max\left\{l_j(s,\dot{s})\right\}$ and $U(s,\dot{s}) = \min\left\{u_j(s,\dot{s})\right\}$ for all $j = 1,2,\cdots,\ell$ for which $\hat{m}_j(s) \neq 0$.

Sought is the optimal motion law $s(t)$ which minimizes the total cycle time t_{f} that the system needs to move from a state $[s_0,\dot{s}_0]^{\mathrm{T}}$ to state $[s_{\mathrm{f}},\dot{s}_{\mathrm{f}}]^{\mathrm{T}}$ without violating the constraints defined by Eq. 14 and Eq. 12.

3.2 Computation of the Dynamic Constraints

All terms in Eq. 11 can be computed at every state $[s_{\mathrm{act}}, \dot{s}_{\mathrm{act}}]^{\mathrm{T}}$ by using the object-oriented approach described in [10]. The residual forces resulting from the computation of the motion and force transmissions, namely

$$\underline{\overline{Q}} = \varphi_S^{D^{-1}}(s, \dot{s}, \ddot{s}) = -\underline{m}(s)\,\ddot{s} - \underline{c}(s, \dot{s}) - \underline{d}(s), \tag{15}$$

can be used to generate $\underline{m}$, $\underline{c}$ and $\underline{d}$ of equation Eq. 10 at every configuration s by the following simplified procedure:

a) Computation of $\underline{d}$: Set, at the input of $\varphi_S^{D^{-1}}$, the configuration to $s = s_{\mathrm{act}}$, the generalized velocity to $\dot{s} = 0$ and the generalized acceleration to $\ddot{s} = 0$. Then, the terms $\underline{m}\,\ddot{s}$ and $\underline{c}$ of Eq. 15 vanish and the residual force $\underline{\overline{Q}}$ obtained at the input is exactly $-\underline{d}$.

b) Computation of $\underline{c}$: Eliminate the term $\underline{d}$ in the calculation of $\varphi_S^{D^{-1}}$ by 'switching off' the gravitational forces $\underline{Q}_{\mathrm{G}}$, and set, at the input of $\varphi_S^{D^{-1}}$, the configuration to $s = s_{\mathrm{act}}$, the generalized velocity to $\dot{s} = \dot{s}_{\mathrm{act}}$ and the generalized acceleration to $\ddot{s} = 0$. Then, the term $\underline{m}\,\ddot{s}$ of Eq. 15 vanishes and the residual force $\underline{\overline{Q}}$ obtained at the input is exactly $-\underline{c}$.

c) Computation of $\underline{m}$: Similarly, eliminate the terms $\underline{c}$ and $\underline{d}$ in the calculation of $\varphi_S^{D^{-1}}$ and set the input acceleration to $\ddot{s} = 1$. Then, the resulting force $\underline{\overline{Q}}$ is exactly $-\underline{m}$.

The generation of the equations of motion by this approach requires 3 traversals of the inverse dynamics $\varphi_S^{D^{-1}}$ for one set of equations.

The Jacobians ${}_{\mathrm{E}}\mathbf{J}_s$ and ${}_{q}\mathbf{J}_s$ of equations Eq. 6 can be computed similarly using the so-called kinematical differentials (see [10]).

3.3 Solution of the Time-Optimal Problem

It can be shown that the time-optimal motion along a given spatial path $\mathscr{P}(s)$ under the above mentioned constraints is composed exclusively of trajectories with maximal or minimal acceleration. Time-optimality implies that the time-optimal motion law $s(t)$ is a monotonically increasing time function, i. e. that the velocity $\dot{s}$ along the trajectory is further constrained by

$$\dot{s} \geq 0 \tag{16}$$

at every configuration s. Eq. 16 and Eq. 12 as well as Eq. 14 form a set of velocity and acceleration limits at every configuration s, which determines an admissible region in the plane $\dot{s} - \ddot{s}$ for each configuration s (see Fig. 4).

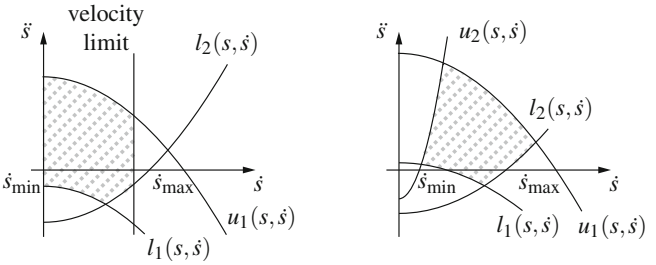

Fig. 4 Admissible acceleration region for given configuration s

If the functions $l_j(s,\dot{s})$, $u_j(s,\dot{s})$ are linear in $\dot{s}^2$, one simple interval $[\dot{s}_{\min},\dot{s}_{\max}]$ of admissible velocities can be defined for every configuration s (Otherwise, the admissible regions may consist of not connected sub-regions leading to a set of not connected admissible velocity intervals.). In this case, the equations Eq. 11 can be written as

$$\hat{\underline{c}}_1(s)\,\dot{s}^2+\hat{\underline{d}}_1(s) \;\le\; \underline{\hat{m}}(s)\,\ddot{s} \;\le\; \hat{\underline{c}}_2(s)\,\dot{s}^2+\hat{\underline{d}}_2(s)\,, \tag{17}$$

the resulting function $G(s,\dot{s})$ (see Eq. 12) is also linear in $\dot{s}^2$, the admissible regions in the plane $\dot{s}-\ddot{s}$ are simply connected, and the set of admissible states has no holes in its interior. This allows for the definition of the functions $\dot{s}_{\min}(s)$ and $\dot{s}_{\max}(s)$ describing the maximally and minimally allowed velocities $\dot{s}$ as a function of the motion coordinate s, called hereafter "lower limiting curve" and "upper limiting curve", respectively. The area between both curves contains the set of admissible states, as shown in Fig. 5.

The states lying on the upper limiting curve $\dot{s}_{\max}(s)$ are classified using Eq. 14 in:

a) sinks, if $U(s,\dot{s})$ and $L(s,\dot{s})$ are defined and

$$U(s,\dot{s})=L(s,\dot{s}) \;>\; \dot{s}_{\max}\,\mathrm{d}\dot{s}_{\max}/\mathrm{d}s\,; \tag{18}$$

b) sources, if $U(s,\dot{s})$ and $L(s,\dot{s})$ are defined and

$$U(s,\dot{s})=L(s,\dot{s}) \;<\; \dot{s}_{\max}\,\mathrm{d}\dot{s}_{\max}/\mathrm{d}s\,; \quad \text{or} \tag{19}$$

c) tangent points, elsewhere.

Moreover, the tangent points at which the velocity constraints described in Eq. 12 are active are called singular points, or singular arcs if they are connected.

The solution to the time-optimal motion is a sequence of branches of maximal acceleration and maximal deceleration which lies in the feasible region and touches tangentially the upper limiting curve. At states $[s,\dot{s}]^{\mathrm{T}}$ lying inside the feasible region, the solution consists of segments with maximal acceleration $U(s,\dot{s})$ and segments with maximal deceleration $L(s,\dot{s})$. At singular points, the maximal acceleration is further bounded by the upper limiting curve tangent $\mathrm{d}\dot{s}_{\max}/\mathrm{d}s$.

With these definitions, the following algorithm based on the one proposed in [5] has been constructed:

Step 0: Check if the initial state s_0 and the final state s_f are feasible for the given initial velocity $\dot{s}_0$ and final velocity $\dot{s}_f$ respectively. If not, the problem has no feasible solution.
Step 1: Set a counter k to 1. Integrate the equation $\ddot{s} = \max\left\{l_j(s,\dot{s})\right\}$ backwards in time from the final state $s = s_f$, $\dot{s} = \dot{s}_f$ until leaving the feasible region. Name the computed deceleration curve $\dot{s}^d(s)$.
Step 2: Integrate the equation $\ddot{s} = \min\left\{u_j(s,\dot{s})\right\}$ forwards in time from the initial state $s = s_0$, $\dot{s} = \dot{s}_0$ until leaving the feasible region. Name the computed acceleration curve $\dot{s}_k^a(s)$. If the acceleration curve $\dot{s}_k^a(s)$ crosses the lower limiting curve $\dot{s}_{\min}(s)$, the problem is not feasible and the algorithm should be terminated. Else, continue.
Step 3: If $\dot{s}_k^a(s)$ crosses the deceleration curve $\dot{s}^d(s)$ terminate the algorithm: the intersection of both curves is the only switching point S_k. Otherwise, continue.
Step 4: Search forwards on the upper limiting curve $\dot{s}_{\max}(s)$ for the next tangent point S_{k+1}. The point S_{k+1} is a switching point candidate.
Step 5: Integrate the equation $\ddot{s} = \max\left\{l_j(s,\dot{s}),\ \dot{s}_{\max}\,\mathrm{d}\dot{s}_{\max}/\mathrm{d}s\right\}$ backwards in time from the state S_{k+1} until crossing one of the acceleration curves $\dot{s}_\ell^a(s)$, with $1 \le \ell \le k$. The intersection of both curves is the switching point S_ℓ. Set $k = \ell$. Disregard the candidates S_r, with $r \le \ell$.
Step 6: Integrate the equation $\ddot{s} = \min\left\{u_j(s,\dot{s}),\ \dot{s}_{\max}\,\mathrm{d}\dot{s}_{\max}/\mathrm{d}s\right\}$ forward in time from the state S_k until leaving the feasible region. Add one to the counter k. Name the computed acceleration curve $\dot{s}_k^a(s)$. If the acceleration curve $\dot{s}_k^a(s)$ crosses the lower limiting curve $\dot{s}_{\min}(s)$, the problem is not feasible and the algorithm should be terminated. Else, go to step (3).

Fig. 5 shows how a typical solution looks like.

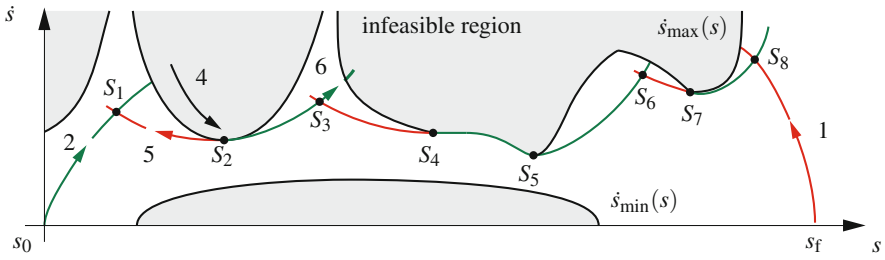

Fig. 5 Time-optimal solution algorithm (no islands)

4 General Waiter Motion Problem

4.1 Waiter Motion Problem along a Given Path

The waiter motion problem considers two set of constraints. One set is given as constant limits in the joint velocities and accelerations $\dot{q}_i^{\min}$, $\dot{q}_i^{\max}$, $\ddot{q}_i^{\min}$ and $\ddot{q}_i^{\max}$,

which are typically provided by the manufacturer and are pre-programmed in the robot controller as soft-limits. A second set is given by the sticking ('no sliding') condition for every object k on the tablet

$$\frac{\hat{\underline{a}}^k \cdot \underline{n}}{\| \hat{\underline{a}}^k \|_2} \geq \cos\alpha\,, \quad \text{with} \quad \hat{\underline{a}}^k = \underline{a}^k + \underline{g}\,, \tag{20}$$

where $\underline{a}^k$ is the acceleration of object k, $\underline{g}$ is the gravity vector, $\underline{n}$ is the normal vector of the tablet plane, and $\mu_0 = \tan\alpha$ is the dry friction coefficient between the tablet and the objects. These k additional dynamic constraints can be rewritten as

$$\sqrt{[\hat{a}_x^k]^2 + [\hat{a}_y^k]^2} \leq \mu_0 \hat{a}_z^k\,, \quad \text{with } \hat{\underline{a}}^k = {}_k\mathbf{J}_s\, \ddot{s} + {}_k\mathbf{J}'_s\, \dot{s}^2 - \mathbf{R}_k^{\mathrm{T}} \underline{g}\,, \tag{21}$$

where ${}_k\mathbf{J}_s$ is the Jacobian mapping the linear velocities $\dot{s}$ along the spatial path to the velocities of object k, and $\mathbf{R}_k$ is the transformation matrix from the inertial frame to the local coordinate frame of object k.

Clearly, equations 21 are nonlinear in the unknowns $\ddot{s}$, which makes their treatment with the previous methods infeasible. However, it is possible to approximate these constraints by replacing the friction cone by a friction polyhedron given by the equations

$$\begin{aligned} &(1) \qquad |\hat{a}_x^k| \;\leq\; \mu_0 \hat{a}_z^k\,, \\ &(2) \qquad \left| \frac{\hat{a}_x^k}{\tan(\varphi_i)} + \hat{a}_y^k \right| \;\leq\; \frac{\mu_0 \hat{a}_z^k \cos(\varphi_1)}{\sin(\varphi_i)}\,, \end{aligned} \tag{22}$$

defined by the discretization angles

$$\varphi_i = \frac{i\,\pi}{2^{p-1}}\,, \quad i = 1, 2, \ldots, 2^{p-1} - 1\,, \tag{23}$$

for each $\hat{a}_z^k$ (see Fig. 6).

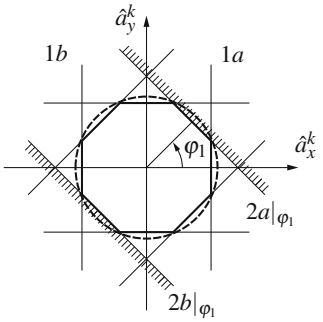

Fig. 6 Cone of friction for $p = 3$

Eq. 22 together with the joint velocity and acceleration limits form a system of constraints which are linear in s^2, so that simply connected admissible acceleration regions are guaranteed. The approximation can be arbitrarily refined by choosing a sufficiently large integer p. Higher numbers p yield better cycle times, though increasing considerably the size of the problem and, hence, the computational effort required to solve it.

The solution for the case of four objects symmetrically distributed on the tablet, a friction polyhedron approximation with $p = 4$, and a given path is shown in Fig. 7.

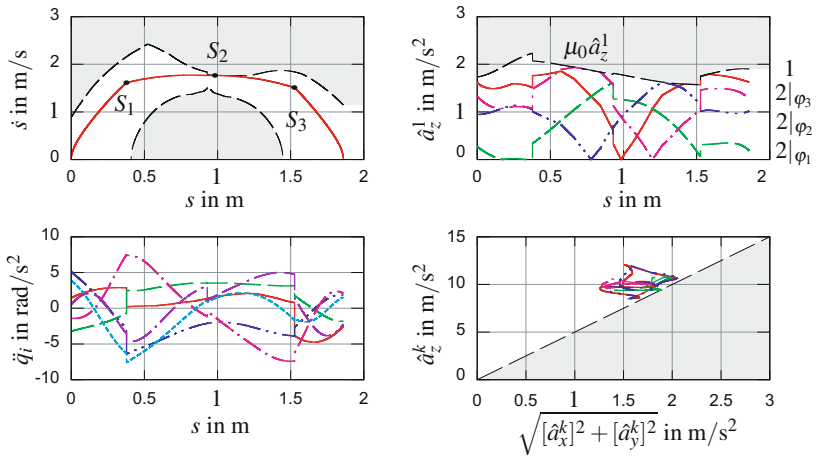

Fig. 7 Optimized waiter-motion along a given trajectory with four objects and $p = 3$ - phase plot, joint accelerations, linearized dry-friction constraints for object 1, and accelerations of all objects

4.2 *Optimization of the Spatial Path Geometry*

The method presented in Sect. 4.1 assigns an optimal cycle time to every feasible spatial path $\mathscr{P}(s; \underline{\zeta})$. allowing for a search for the optimal set $\underline{\zeta}^\star$ of parameters yielding the smallest cycle time. In order to reduce the search space to significant physical subspaces, we propose to define the set of optimization parameters

$$\underline{\xi} = \left[\underline{\varphi}^{\mathrm{T}}, \underline{\beta}^{\mathrm{T}}, \Delta\theta_{z0}^{\mathrm{T}}, \Delta\theta_{z\mathrm{f}}^{\mathrm{T}}, \Delta\underline{\rho}_y\right]^{\mathrm{T}}, \tag{24}$$

where $\underline{\xi}$ describes the geometry of the spatial path $\mathscr{P}(s; \underline{\zeta})$ with respect to a reference geometry $\mathscr{P}(s; \underline{\zeta}_0)$. Vector $\Delta\underline{\rho}_y$ collects m center-line via-point displacements in transversal direction $\underline{e}_{y\,j}$, so that the modified via-points are defined as

$$\underline{p}_j = \underline{p}_j(\underline{\zeta}_0) + \Delta\rho_{y\,j} \cdot \underline{e}_{y\,j}(\underline{\zeta}_0) \quad \forall j = 1, 2, \ldots, m. \tag{25}$$

The angles $\Delta\theta_{z0}$ and $\Delta\theta_{zf}$ describe $m_t = 2$ displacements in the first-order boundary conditions such that

$$\underline{t}_0 = \mathtt{Rot}\,[z, \Delta\theta_{z0}] \cdot \underline{t}_0(\underline{\zeta}_0) \tag{26}$$

$$\underline{t}_f = \mathtt{Rot}\,[z, \Delta\theta_{zf}] \cdot \underline{t}_f(\underline{\zeta}_0)\,, \tag{27}$$

where $\underline{t}_0$ and $\underline{t}_f$ are the tangents of $\Delta\underline{r}(s)$ at its beginning and its end, respectively. Finally, $\underline{\beta}$ and $\underline{\varphi}$ collect m_β and m_φ via-angles describing rotations about the tangential and normal directions of the DARBOUX frame, respectively.

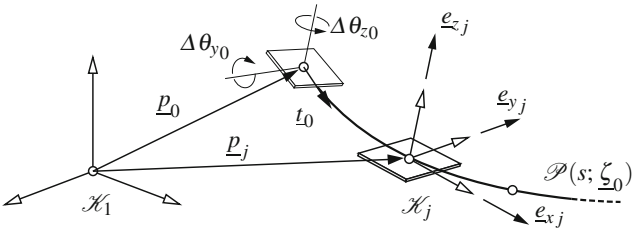

Fig. 8 Spatial path design parameters

The optimization problem is stated as

$$\begin{aligned} &\text{minimize} \\ &\qquad F\,(\underline{\xi}) \;= t_f\,, \end{aligned} \tag{28}$$

where t_f is the optimal cycle time along the spatial path $\mathscr{P}(s;\underline{\zeta})$ as computed in Sect. 2. If $\mathscr{P}(s;\underline{\zeta})$ is not feasible, $F\,(\underline{\xi})$ is set to a very large number. The fineness of the optimization subproblems is improved by increasing the number of via-points m_β, m_φ and m. Each subproblem uses the results of the previous one as an initial guess and reference geometry and is repeated until no significant improvement of the cost function is achieved. The algorithm stops when neither a further attempt to solve a subproblem nor a refinement of the optimization parameters yields a cost improvement greater than the optimization tolerance.

Table 1 and Fig. 9 show the results for the case of a KUKA robot KR-15-2 carrying a tablet with 4 objects between two given tablet poses for a cone of friction approximation with $p = 4$. One can clearly see that the optimal solution is "pressed" almost during 50% of the path length to the constraint boundary (second plot of Fig. 9). This is an interesting behavior showing that, at least in this case, the optimal path shape also forms the constraint boundary such that it minimizes the area between optimal-time trajectory and upper limit curve (compare to Fig. 7, where the boundary is much more "ragged"). Moreover, one can appreciate the low curvatures of the solution path in target space. This shows that spatial path optimization in task space indeed allows for restricting the optimization search to lower-dimensional

Table 1 Multistep computation of the general waiter-motion problem with $p = 4$, with B-splines of degree $k = 3$ and the NAG routine `e04unc` (`dt` $= 1.0e^{-4}$, `relTol` $=$ `absTol` $= 1.0e^{-10}$, `ds` $= 1.0e^{-4}$, `optimTol` $= 2.0e^{-2}$, `fPrec` $= 1.0e^{-2}$, `cDiffInt` $=$ `fDiffInt` $= 1.0e^{-3}$, `stepLimit` $= 2.0e^{-2}$), on a processor Intel(R) Core(TM) i7-950 @ 3.07GHz

step	m_β	m_φ	m_t	t_f (s)	CPU (s)	
initial	2	2	-	-	2.0985	-
1 (2 ×)	2	2	-	-	1.6411	2872.41
2 (1 ×)	2	2	1	2	1.6409	483.70
3 (1 ×)	5	5	2	2	1.6404	1083.57

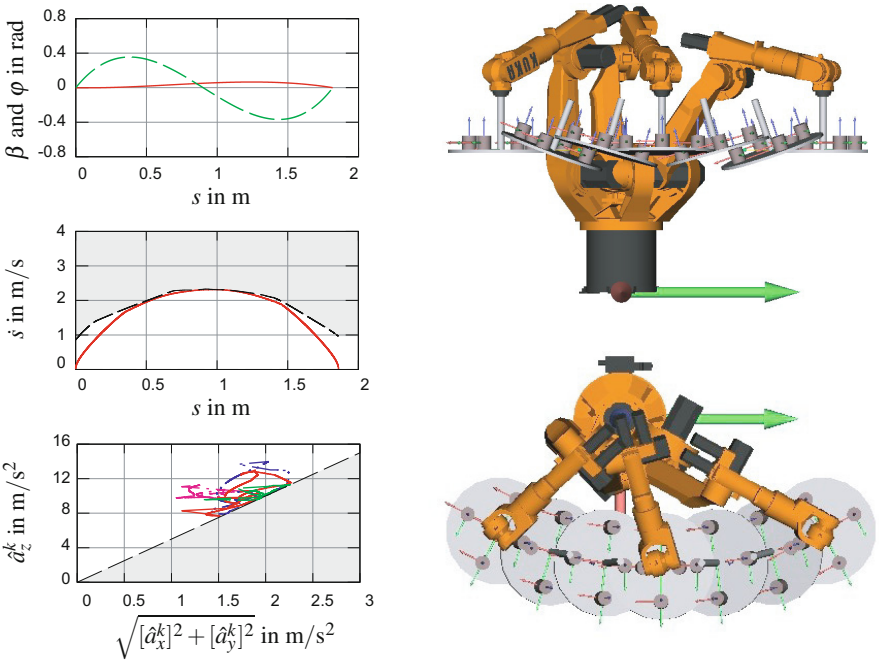

Fig. 9 Optimized waiter-motion along free trajectory with four objects and $p = 3$ - tablet orientation, phase plot and acceleration of all objects

significant subspaces. Table 1 shows the progress of the optimization search for a sequence of subproblems of increasing fineness. The first row shows the cycle time for an initial, slightly curved tablet displacement with purely horizontal attitude. The second row shows the results for the first subproblem: the optimization of the orientation of the tablet, which yields a cycle time improvement of 22%. The third and fourth lines show the results of the final subproblems, in which, in addition to orientation optimization, curve bending is allowed by setting free the two boundary

tangents as well as one and then two via points, respectively. One can see that the last optimization yields only marginal improvements while consuming substantial CPU time. Altogether, the example shows that advantages may exist for certain applications when using task space coordinates for describing and shaping the optimal path instead of using joint coordinates.

5 Conclusions

In conclusion, the paper shows that the so-called general waiter motion problem — which is akin to several industrial problems in which tangential forces are restricted due to functional reasons — can be solved by decomposing the overall optimization problem into two cascaded optimization components: shaping the optimal geometry of the spatial path, and finding the time optimal one-dimensional motion of the system along this path. By parametrizing the spatial path using via poses in SE(3), a more natural and lower-dimensional search space could be obtained, improving the convergence behavior of the optimizer. Subdividing the problem in a sequence of cost functions and search spaces of increasing fineness yielded convergence, which was not possible by direct optimization. The completion of the method involved describing spatial motion by quintic and cubic B-Spline curves for translation and rotation, respectively, as well as the extension of the well-known time-optimal algorithm from robotics in three directions: (1) formulating it in an object-oriented multibody framework, (2) allowing for no-slip conditions to be considered, and (3) introducing the concept of a lower limiting curve in order to handle spatial paths for which some configurations are not feasible at rest.

Future research will focus on extending the method to more general types of constraints. Of special interest for robotic applications is the limitation of motor jerks as well as the consideration of non-conservative effects such as sliding friction and discontinuities caused by impacts. Moreover, genetic algorithms will be tested, in particular for generating better initial-value guesses.

References

1. Gasparetto, A., Zanotto, V.: Optimal trajectory planning for industrial robots. Advances in Engineering Software 41(4), 548–556 (2010)
2. Rana, A., Zalzala, A.: An evolutionary planner for near time-optimal collision-free motion of multi-arm robotic manipulators. In: UKACC International Conference on Control, vol. 1, pp. 29–35 (1996)
3. Bobrow, J.E., Dubowsky, S., Gibson, J.S.: Time-optimal control of robotic manipulators along specified paths. The International Journal of Robotics Research 4(3) (1985)
4. Pfeiffer, F., Johanni, R.: A concept for manipulator trajectory planning. IEEE Journal of Robotics and Automation 3, 115–123 (1987)
5. Shiller, Z., Lu, H.-H.: Robust computation of path constrained time optimal motions. In: Proceedings of the IEEE International Conference on Robotics and Automation, Cincinnati, OH, USA, vol. 1, pp. 144–149 (1990)

6. Geu Flores, F., Kecskemethy, A., Poettker, A.: Time-optimal motion planning along specified paths for multibody systems including power constraints and dry friction. In: Proceedings of the Multibody Dynamics 2011, Brussels, Belgium, July 4-7 (2011)
7. Geu Flores, F.: An Object-Oriented Framework for Spatial Motion Planning of Multibody Systems. Ph.D. thesis, Duisburg (2012)
8. Tändl, M., Kecskeméthy, A., Schneider, M.: A design environment for industrial roller coasters. In: CD Proceedings of the ECCOMAS Thematic Conference on Advances in Computational Multibody Dynamics, Milano, Italy, June 25-28 (2007)
9. Dierckx, P.: Curve and Surface Fitting with Splines. Clarendon Press, Oxford (1993)
10. Kecskeméthy, A., Hiller, M.: An object-oriented approach for an effective formulation of multibody dynamics. CMAME 115, 287–314 (1994)